ARMY RESEARCH LABORATORY

Remote Netted Acoustic Detection System:

Final Report

by Nassy Srour
Army Research Laboratory
and
James Robertson
IIT Research Institute

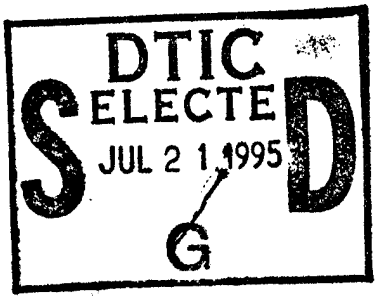

ARL-TR-706 May 1995

Approved for public release; distribution unlimited.

JGK

The findings in this report are not to be construed as an official Department of the Army position unless so designated by other authorized documents.

Citation of manufacturer's or trade names does not constitute an official endorsement or approval of the use thereof.

Destroy this report when it is no longer needed. Do not return it to the originator.

Preliminary copy

REPORT DOCUMENTATION PAGE

Form Approved
OMB No. 0704-0188

1. AGENCY USE ONLY *(Leave blank)*	2. REPORT DATE	3. REPORT TYPE AND DATES COVERED
	May 1995	Final, from Feb 1992 to Sept 1994

4. TITLE AND SUBTITLE
Remote Netted Acoustic Detection System: Final Report

5. FUNDING NUMBERS
DA PR: DC10
PE: P65

6. AUTHOR(S)
Nassy Srour (*Army Research Laboratory*) and James Robertson (*IIT Research Institute*)

7. PERFORMING ORGANIZATION NAME(S) AND ADDRESS(ES)
U.S. Army Research Laboratory
Attn: AMSRL-SE-EA
2800 Powder Mill Road
Adelphi, MD 20783-1197

8. PERFORMING ORGANIZATION REPORT NUMBER
ARL-TR-706

9. SPONSORING/MONITORING AGENCY NAME(S) AND ADDRESS(ES)
U.S. Army Research Laboratory
2800 Powder Mill Road
Adelphi, MD 20783-1197

10. SPONSORING/MONITORING AGENCY REPORT NUMBER

11. SUPPLEMENTARY NOTES
AMS code: 665604C1011
ARL PR: 33E030

12a. DISTRIBUTION/AVAILABILITY STATEMENT
Approved for public release; distribution unlimited.
Preliminary copy.

12b. DISTRIBUTION CODE

13. ABSTRACT *(Maximum 200 words)*

A Remote-Netted Acoustic Detection System (RNADS) has been developed at the U.S. Army Research Laboratory for the detection of ground and air targets in a typical battlefield environment. The system involves non-line-of-sight (NLOS), real-time *x-y* coordinate tracking, detection, and classification of targets at tactical ranges. The acoustic detection system includes a set of microphone arrays, surveyed a few kilometers apart and networked together through a radio link. Each microphone array is connected to a signal processing box that determines the line-of-bearing (LOB), frequency, time, signal-to-noise ratio (SNR), and classification of detected targets. The data from each sensor array are transmitted to a central processing station, where a multiple hypothesis tracking (MHT) algorithm and a Kalman filter tracking algorithm are used to calculate and track the real time *x-y* coordinates of detected targets. The information is in turn overlayed on a digitized map of the terrain. A series of field experiments was conducted to evaluate the performance and capability of the system.

14. SUBJECT TERMS	15. NUMBER OF PAGES
Acoustic detection, tracking, classification	41
	16. PRICE CODE

17. SECURITY CLASSIFICATION OF REPORT	18. SECURITY CLASSIFICATION OF THIS PAGE	19. SECURITY CLASSIFICATION OF ABSTRACT	20. LIMITATION OF ABSTRACT
Unclassified	Unclassified	Unclassified	UL

NSN 7540-01-280-5500

Standard Form 298 (Rev. 2-89)
Prescribed by ANSI Std. Z39-18
298-102

Preface

A Remote-Netted Acoustic Detection System (RNADS) has been developed at the U.S. Army Research Laboratory for the detection of ground and air targets in a typical battlefield environment. A series of field experiments was conducted to evaluate the performance and capability of the system.

The following agencies contributed to the success of the RNADS program.

RNADS Development Team:

- U.S. Army Research Laboratory (ARL)
  2800 Powder Mill Road
  Adelphi, MD 20783-1197
- U.S. Army Armament Research, Development, and Engineering Center (ARDEC)
  Picatinny Arsenal, NJ 07806-5000
- U.S. Army Communications-Electronics Command (CECOM)
  FT Monmouth, NJ 07003-5000
- IIT Research Institute (IITRI)
  4140 Linden Avenue, Suite 201
  Dayton, OH 45432
- LICA Systems, Inc.
  10400 Eaton Place, Suite 312
  Fairfax, VA 22030
- SenTech, Inc.
  5 Militia Drive, Suite 105
  Lexington, MA 02173

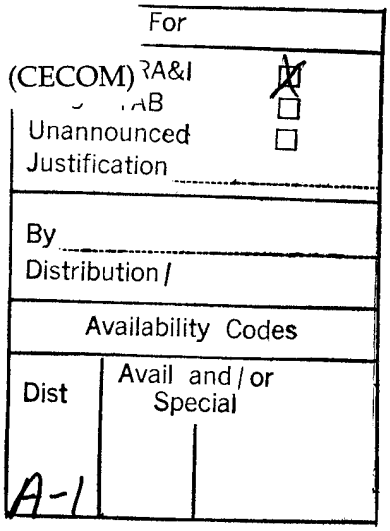

ARL acted as the program manager, ARDEC provided the sensor for the air targets, and CECOM contributed the low-cost packet radios.

SenTech, Inc., provided the sensors for the ground targets, LICA, Inc., contributed multiple hypothesis tracking (MHT) linear Kalman filter, and IITRI also provided MHT, as well as coordination on the extended Kalman filter test.

Contents

Figures

1. Introduction

The acoustic emissions of ground vehicles, helicopters, and aircraft can be passively detected without the line-of-sight restrictions of radar and optical systems. A wealth of information can be extracted from acoustic sensors including target range and velocity, target direction and classification, and the presence of multiple targets. When compared to radar and optical systems, acoustic sensors are inexpensive. With the proper environmental conditions, a high signal-to-noise ratio (SNR) is obtainable. The acoustic emissions of targets are also difficult to disguise. Attempts to reduce target noise often result in an undesirable loss in performance. These characteristics of acoustic technology make developing systems for monitoring targets within a battlefield using acoustic sensors attractive. Acoustic sensing will complement existing techniques used for target acquisition and battlefield intelligence.

A brief discussion of the sources of acoustic emissions provides an understanding of the processing needed within an acoustic sensor. A general description of the feature data extracted from broad classes of targets provides a basis for differentiating the spectra of helicopter, aircraft, and ground vehicles.

The principal acoustic sources of a helicopter are the main and tail rotor systems, and the engine. The fundamental frequency and harmonics are easily located upon observation of the power spectrum of a helicopter. The main rotor is generally easier to locate than the tail rotor. Systems will often use the relationship between the main rotor frequency and the tail rotor frequency for identification. In contrast to helicopters, jet engines in aircraft lack characteristic harmonic trains. They contain a broadband energy distribution with some individual strong frequency lines.

Ground vehicles may have considerable harmonic content. Their acoustic emissions contain a combination of random and periodic components. Noise is produced from the propulsion systems (e.g. engine, exhaust), tires, and tracks. A narrowband analysis will show characteristic peaks at frequencies related to a source such as the cylinder firing rate, engine firing rate, and turbine rotor blades. For cylinder base engines, the engine firing rate is usually the most predominant line in the spectrum. Turbine engines produce no fundamental firing rate; therefore, the acoustic energy is relatively flat and evenly distributed across the low frequencies. Tire noise of trucks and wheeled vehicles results from the interaction between the tires and the road surface. This noise source may be attributed to tire vibration, and the entrapment and subsequent release of air from the tread cavities.

Some tracked vehicles may have a high-frequency peak associated with the sprocket and track system. As the tank moves, the track pulls from side to side, causing the center guide to scrape against the steel rim of the road wheels. This steel-to-steel scraping causes the center guide to vibrate at its resonance frequency.

Engine accessories such as pumps, fans, generators, and auxiliary motors will produce discrete frequency components. Adequate vehicle design information is needed in order to properly identify these sources; however, accessories are not usually harmonically related to other engine frequency lines, and accessory frequency lines are usually weaker in amplitude and higher in frequency than the cylinder firing rate.

The detection of acoustic signals is not without its limitations. Difficulties arise from the signature variabilities caused by variation in ground vehicle rpm, environmental conditions, and reduced propagation distances associated with a source close to the surface. Noise differences may also be attributed to vehicle speed, the load being carried, and the level of maintenance. Meteorological conditions and their effect on acoustic sensor performance will be discussed in the following section.

1.1 Meteorological Conditions and Acoustic Sensor Performance

The performance of acoustic sensor systems has been observed to vary widely through the diurnal cycle, being at its best at night and at its worst at midday. These variations in performance can be traced to changes in meteorological conditions that affect both acoustic propagation and the background noise levels.

The performance of an acoustic sensor is ultimately determined by the SNR available at the processing system before various processing techniques are applied to improve the quality of the signal. The SNR is expressed by the passive sonar equation

$$SNR = SL - TL - NL \ , \tag{1}$$

where SL is the source level, TL is the transmission loss, and NL is the background noise level. Both TL and NL are determined by the meteorological conditions at the test site. Transmission losses depend on how well the acoustic waves propagate through an atmosphere stratified by changes in temperature and wind velocity. Noise levels (those not caused by man-made or cultural sources) are caused by the turbulent flow of air over the microphones.

1.1.1 Acoustic Propagation Losses

As sound waves travel through the atmosphere, they are refracted up or down by changes in the sound velocity profile (SVP). The SVP is determined by the variations of temperature and wind velocity as a function of height, and these are likely to change through the course of the day.

The best propagation conditions occur at night, when the lower levels of the atmosphere are colder than the upper levels. This produces a positive gradient in the SVP, a condition that causes sound waves to bend downward, making it easier for them to travel from source to receiver. An oppo-

site condition occurs during the day, when the lower levels of the atmosphere become warmer than the upper levels. The result is a negative gradient in the SVP, a condition that causes sound waves to bend upward, making it more difficult for them to travel from the source to the receiver. In some conditions, the degree of bending is such that sound waves cannot reach the receiver other than indirectly, after being scattered by upper-air turbulence. This is called a shadow zone.

Diurnal effects are more pronounced in the desert, where the lack of vegetation and clear dry air make the cycle of heating and cooling of the ground and the lower levels of the atmosphere more pronounced.

With the use of a propagation model, the propagation losses (TL) can vary by up to 15 dB between the hours of 5:00 a.m. and 1:00 p.m. solely on the basis of changes in the temperature profile (without the sensor being in the shadow zone).

1.1.2 Background Noise Levels

When set up outdoors, microphones are always protected by windscreens; nevertheless, wind noise still significantly limits the performance of the acoustic sensors. Wind noise originates in two ways: First, turbulence is created downstream from the windscreen, generating pressure variations that are indistinguishable from acoustic noise; second, turbulence generated upstream from the windscreen (from vegetation, thermals, etc) is convected past the microphones, generating pressure variations that are recorded as noise. Of these two effects, the latter is by far the more important. The random pressure fluctuations induced by flow are not propagating sound waves, so their effect decays exponentially as the distance from the microphone to the surface of the windscreen increases. Size, therefore, is the best quality in a windscreen, overshadowing shape or choice of materials.

In the absence of storms or other unusual phenomena, winds near the surface decrease substantially at night and become less turbulent. This reduces the background noise level considerably, a factor which further explains the improved performance of acoustic sensors during the night.

Considering the effects of propagation and background noise levels as quantified in the passive sonar equation, we expect to see substantial differences in the performance of an acoustic sensor at different times of the day. Fortunately, variations in the performance level of acoustic surveillance sensors is in line with requirements for their use in tactical situations. Night reduces the utility of visual sensors, just when the threat of surprise attacks is greater. Under these conditions, acoustic sensors, operating at their maximum level of performance, are likely to yield the most benefits.

1.2 Remote Netted Acoustic Detection System (RNADS) Concept

The Army Research Laboratory (ARL) has developed a Remote Netted acoustic detection system (RNADS) for the detection of ground vehicles and air targets. RNADS is composed of acoustic sensor arrays placed in the battlefield, a network-control processing facility outside of the battlefield, and a radio link from the remote sensors to the network control. RNADS monitors movement over an area of interest by detecting the acoustic emissions of vehicles and air targets. Once the target is detected, the sensors determine and transmit the target's line of bearing relative to the sensor, along with other pertinent information, to the network control where processing is performed to determine the target track. The system is capable of tracking multiple targets in real time. Figure 1 illustrates the functionality of RNADS. This report documents the development and testing of RNADS.

1.3 RNADS Objectives

The objectives of the RNADS program are to

- evaluate and enhance acoustic sensor algorithms in a multi-target environment;
- evaluate and enhance tracking algorithms in a multi-target environment;

Figure 1. RNADS functionality.

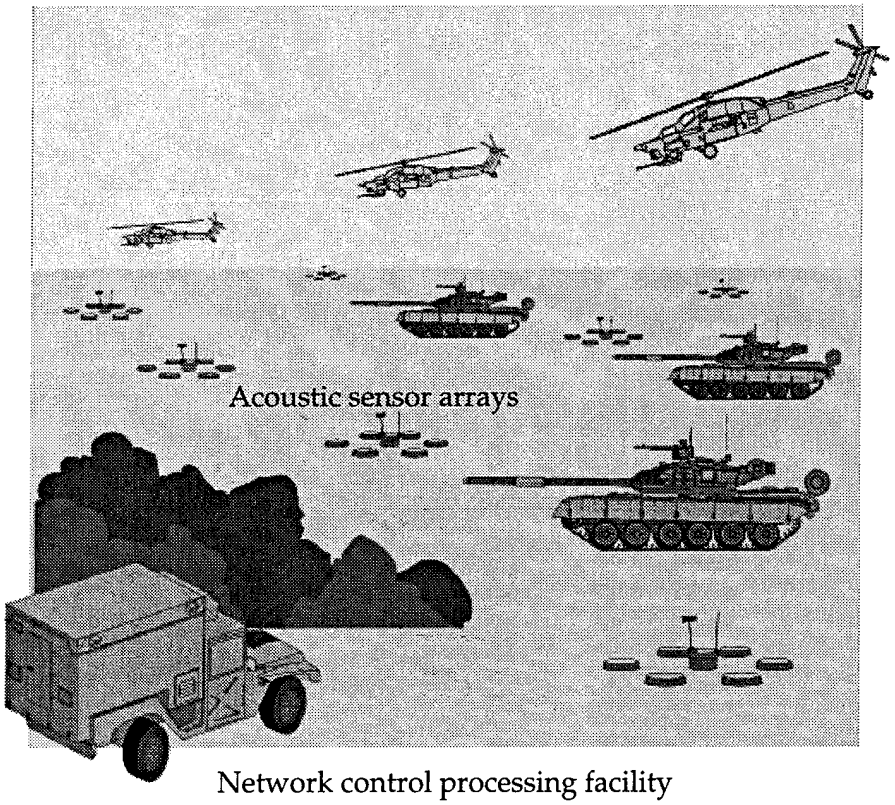

- demonstrate passive target tracking in real time in a multi-target environment; and
- increase the database of acoustic signatures.

To satisfy these objectives, a team of government and contractor personnel was formed, sponsored by the ARL Advanced Technology Management Organization. A rigorous research, development, and testing program was initiated to complete the project on time and demonstrate passive acoustic x-y tracking in real time during an Israeli field exercise, as part of a cooperative technology exchange program between the U.S. and Israel.

2. RNADS System Overview

RNADS comprises a number of remote acoustic sensors, a network control facility, and communications processors (CPs). The main function of the remote sensor is to detect targets within the sensor's field of regard and calculate target direction relative to the sensor. This information is then packetized and sent, using the CP, to the network control processing facility. A low-cost packet radio (LPR) was used to transmit the data packets. An HDLC interface provides bidirectional communications between the remote site and the network-control processing facility. At that facility, tracking algorithms associate multiple lines of bearings to generate target tracks. These tracks are displayed on a Sun workstation, along with terrain and other information. A meteorological station, which collects wind speed, wind direction, temperature, barometric pressure, and relative humidity, is placed at most remote sites. Figure 2 shows an overview of the RNADS system.

2.1 Sensor Architecture

The RNADS sensors are passive acoustic sensors designed to detect, localize, track, and classify ground and air vehicles at medium to long ranges. The architecture of the RNADS sensors was derived from the advanced passive sonar systems used by the U.S. Navy.

Each remote sensor site consists of an acoustic sensor processing unit and associated microphones, a Global Positioning System (GPS) receiver, a digital audio tape (DAT) recorder, an LPR, and a CP. The CP provides the interface between all sensor site elements.

The sensor transducer array consists of a seven-element circular array of microphones connects to a preamplifier box. A 100-ft-long multi-conductor cable connected the preamplifier box to the processing unit, implemented on a rugged, transportable personal computer (PC). The PC contains an anti-aliasing filter board, an analog-to-digital converter board (A/D), and a digital signal processing (DSP) board. State-of-the-art signal processing algorithms were implemented in C to perform the required functions.

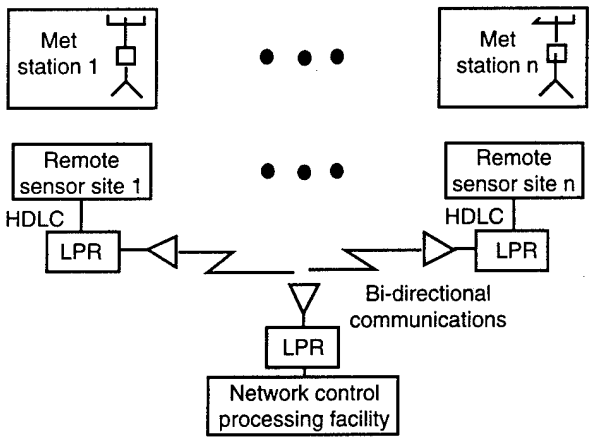

Figure 2. RNADS system overview.

The sensor prepared messages containing the estimated target bearing, the frequencies of the main peaks, and the target types, and passed these messages to a CP over an RS232 interface. The CP distributed the data through the network using LPRs. Both ac and dc options are available for supplying power to the remote sensor. Figure 3 shows the remote site components, which include the sensor and CP. The remainder of this section will describe the sensor system hardware, algorithms, and software.

2.1.1 *Acoustic Sensor Hardware*

The hardware architecture for the acoustic sensor is shown in figure 4.

The acoustic sensor array used Knowles BL1994 ceramic microphones. They are rugged, inexpensive, instrumentation-quality transducers. The sensing array consisted of seven microphones—six forming a circle with the seventh in the center. The circle had a diameter of 8 ft. The size of the array was chosen to provide good directivity at the lower frequencies. The number of microphones was determined by the number of channels in the A/D converter (eight) and the desire to keep the computational load at a low level. The microphones were placed on aluminum spikes driven into the ground. The spikes were positioned with the aid of a jig with a built-in magnetic compass.

The microphones were covered by open-cell foam windscreens 6 in. in diameter. The windscreens were originally gray, and when they were placed near the ground in low grass, they were hard to detect from a distance. Ex-

Figure 3. Remote sensor components.

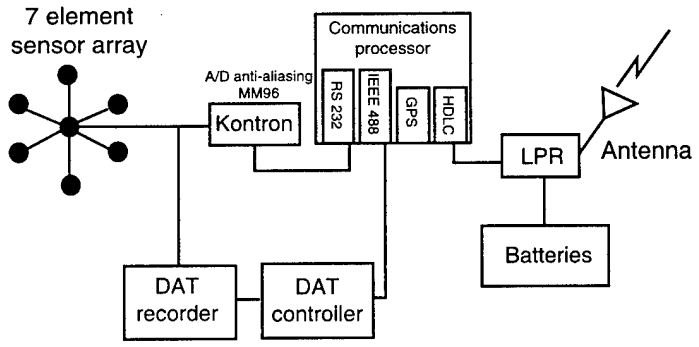

Figure 4. RNADS acoustic sensor hardware architecture.

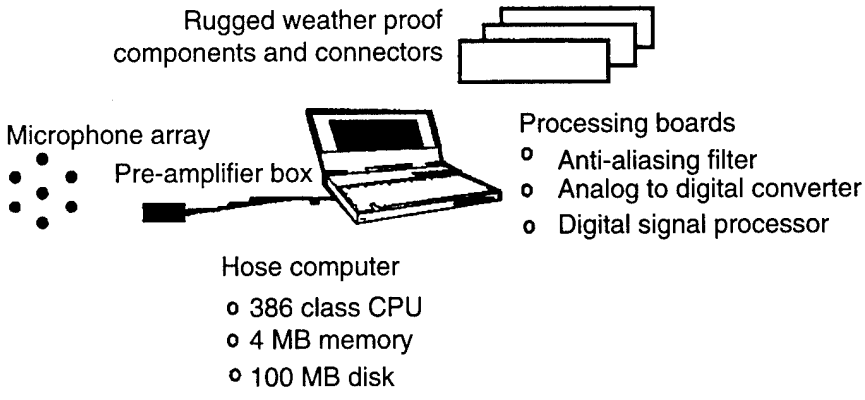

posure to sunlight changed the color to an olive green, making visual detection even more difficult. The acoustic properties did not seem to be affected.

The preamplifier box had two functions: It provided power to the microphones (5 V), and amplified signals from eight channels before sending them over the cable to the processor. Having preamplifiers for all eight channels proved useful on several occasions when there was electrical trouble in one of the preamplifier boxes or cables. We were often able to bypass the difficulty by using the spare channel and reconfiguring the array in software. The preamplifier circuit could provide switch-selectable gains of 40 and 60 dB. The preamplifier boxes could get power from three 9-V batteries or through the cable from the filter card.

The cable had 16 shielded wires and was 100 ft long. Eight signals, a ground, and ±12 V ran through the cable. The end connecting to the preamplifier was a 16-pin circular connector; the other end had a DB-25 (RS-232 type) connector, which could be connected to the filter board in the ruggedized PC, to a digital tape recorder, or with a short ribbon cable jumper to both.

The filter board was a half-size PC card that fit into the ruggedized PC. It had eight 4-pole, 300-Hz lowpass filters (frequency devices 796BT-4, 300 Hz) and a module to convert 12 V from the PC's bus to isolated ±12 V for the filters and the preamplifier box. Signals are sent from the filter board to the A/D converter via a 50-wire flat cable.

The A/D converter was a commercially available, 16-bit system with simultaneous sample-and-hold (data translation DT2809). The simultaneous sample and hold (SS&H) feature captures data from all channels at the same time. This simplifies the software by eliminating the need to compensate for sampling delays between channels.

The DSP board was a commercially available board (Ariel MM-96) that had two Motorola 96002 DSP chips, 192K words of static random-access memory (RAM) and 1 Mword of dynamic RAM.

2.1.2 *Sensor Software*

The software for the RNADS sensor may be divided into development and distribution software suites. The development software suite includes the Intermetrics and Microsoft C compilers, the Ariel C Demo software, and a number of developed utilities for hardware debugging and data reduction. The distribution software suite has the source and executable code for both the PC and Ariel board, as well as data files specifying the sensor array, the overall configuration, and the target classifier data.

The software for the Ariel board is written in Intermetrics C. The fast Fourier transform (FFT) routine is written in Assembly language. Currently, all the code runs on one of the two DSP chips (DSP A). The program is stored in the "outer static RAM"; the data are in the "inner static and dy-

namic RAMs." This change from earlier versions, where almost everything is stored in the inner RAMs, results in substantially faster run cycles (about a factor of two), but has pushed the information stored in the outer RAM to more than 16 Kwords, necessitating the use of 64-K static RAMs.

The Ariel board software takes data from the PC program and converts it into line-of-bearing data. Spectrum data are generated and sent to the PC. The general program flow is shown in figure 5.

The following are descriptions of each of the data flow blocks shown in figure 5.

Input.—Data from seven microphones are sampled at 1024 Hz and used as input.

2048-point FFT spectra.—Each channel of data is Hamming windowed and fed through the FFT. The time-versus-frequency plot is displayed on the PC.

Beamforming.—Currently 12 beams, equally spaced around the circle, are defined; for every frequency between the low- and high-beamformer frequencies (20 to 250 Hz), a magnitude in the beam direction is calculated. The beam calculation may be done using a delay sum or a singular value decomposition (SVD) beamformer. For any desired frequency, the bearing is determined by applying a centroid over the strongest beam and adjacent beams. The number of beams and low and high frequencies, as well as the beamformer type, are selectable in the parameter files. A time-versus-azimuth plot is also displayed on the PC.

Peak picking and HLA.—A frequency peak has an amplitude that is a specified amount higher than other peaks in its neighborhood. Three peak pickers, median, Wiener, and histogram, are available and selectable through the configuration files. Each generates a list of frequency peaks.

Harmonic line set (HL set).—The HL set is a set of frequency peaks that are harmonically related to each other. The harmonic line association (HLA) algorithm takes the strongest peak, *P*, in the frequency peak list and, subject to some constraints, assumes that it is the *k*th harmonic of a

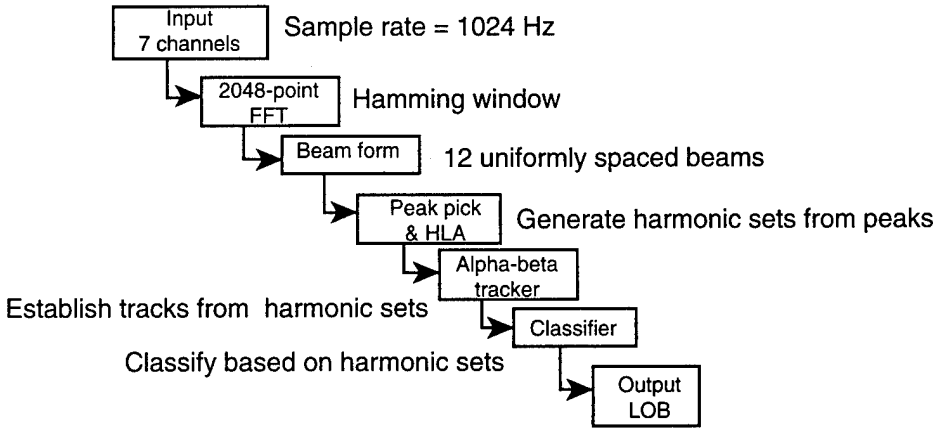

Figure 5. RNADS sensor software data flow.

fundamental frequency, F ($P = k*F$); then the total signal strength in the HL set is calculated. The k that gives the maximum signal strength is assumed to be correct. A set of features corresponding to the signal strength in decibels is generated. The process is repeated for any peaks that have not been used.

Generate tracks.—The strongest HL set is assumed to be associated with a target. If weaker HL sets are close enough in bearing, they are assumed to be associated with the same target (for example, the HL sets associated with engine noise and track noise in a tank). After this simple combining of HL sets is done, the HL sets are associated with tracks. There are three associators, selectable from the parameter files:

- *Dummy associator.* Each HL set is reported as a track. This eliminates "track history," but may be desirable for testing, or if there is a powerful multisensor fusion algorithm elsewhere in the system.
- *Alpha-beta associator.* The track bearing is projected ahead using an alpha-beta tracker. The HL set nearest to the projected position is associated with the track.
- *MAP associator.* The track bearing is projected ahead using a maximal a posteriori (MAP) tracker. The HL set nearest to the projected position is associated with the track.

Assign target classes.—The track maintains a list of features (decaying exponential filter on the feature data in the associated HL set), which is fed into a classifier (currently a quadratic log likelihood estimator is used). The target class that best fits the track features is reported.

Generate and send out lines of bearing (LOBs).—The LOB structures are filled in from track data and the Ariel board tells the PC that the LOB data are ready.

2.2 Network Control Architecture

The RF communications link between the remote sensor sites and the network control processing facility (NCPF) is via an AN/PRC118( ) LPR. The LPR uses the Survivable Radio Network (SURAN) protocol to ensure reliable communications between all nodes in the network. The LPR receives packets of data from an attached device (i.e., remote site CP or NCPF), via an HDLC link. The LPR transmits the packet in a spread-spectrum signal at either 400 Kbps or 100 Kbps to a neighboring LPR. The receiving radio, upon receiving a good packet, will transmit an acknowledgment back to the transmitting station. If no acknowledgment is received, the packet will be retransmitted. Any LPR in the network can be used as a relay if point-to-point communications are not possible.

2.2.1 Communications Architecture of Remote Sensor Sites

The CP performs many functions. Its primary function is to collect LOB reports from the acoustic sensor, packetize them into a format acceptable to

the LPR network, and finally to transmit the packets via the HDLC card and the LPR network to the NCPF. In addition to this task, many others need to be performed by this element. It must periodically collect information from the GPS receiver in order to ascertain the location of the node, as well as the current time. It must send this time back to the acoustic sensor in order to maintain an accurate time within the sensor's processor. The location of the node must be packetized and transmitted to the NCPF. Finally, the CP must also be capable of receiving a request, via the LPR network, from the NCPF.

The received message will be directed to the DAT recorder, acoustic sensor, or to the CP. Commands to the DAT can include any command available through the attached GP-300/GP-301. These commands include but are not limited to: RECORD, STOP, PAUSE, SEARCH for COUNTER EVENT, REQUEST COUNTER VALUE, etc. Commands to the CP include instructions to get a new GPS fix and to reboot the acoustic sensor. Commands to the acoustic sensor will include instructions to load new software or change parameters on the current software. All commands can be set to be executed immediately or at some time in the future. The CP operates as a diskless system booting from erasable programmable read-only memory (EPROM) stored MS DOS. The entire communications processing and interface software, developed in C, is loaded, in executable form, into the CP EPROMs. The CP software includes a "watchdog" program that reboots the system if the software "hangs up" or there is an interruption of power.

The NCPF consisted of a CP and four SUN SPARCstations. A schematic of the NCPF is shown in figure 6. The NCPF is interfaced to the network via a CP that is identical in function to the sensor site CP. The NCPF CP does not include a GPS receiver or IEEE 488 interface card. The NCPF software functions are split between a SPARCstation II and a SPARCstation 10 for the tracker and software. The SPARC 10 is used for sensor data processing, while the SPARC II provides the display processing and generation and system control function. The NCPF uses the UNIX concept of "sockets" and "pipes" to move data between the two SUN SPARCstations. The remaining SPARCstations, a SPARC 1+ and SPARC 2, were used by IIT Research Institute (IITRI) for tracking, display, and data logging.

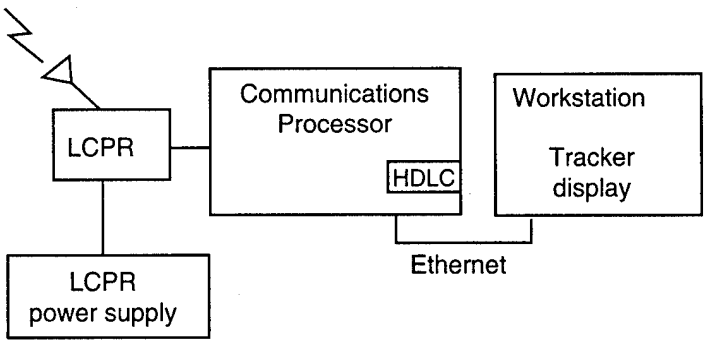

Figure 6. Network control processing facility.

2.3 Tracking Algorithms

A number of tracking algorithms were developed to interface with the RNADS. The tracker combines information received from every sensor array and generates tracks related to detected targets. One tracker uses a multiple-hypothesis data association logic and a linear Kalman filter for fix incorporation. Another uses multiple-hypothesis logic and an extended Kalman filter for fix incorporation. A third tracker that was developed uses a nearest-neighbor data association algorithm and an extended Kalman filter. In this section we describe the tracking algorithms.

2.3.1 *Acoustic Tracker Using Multiple Hypothesis Logic and Linear Kalman Filter*

This tracker uses a multiple hypothesis tracker (MHT), which consists of two correlation processes in tandem. The first correlation process, on a scan-by-scan basis, correlates pairs of lines of bearing received from acoustic sensors and generates measurement data points. Each data point generated consists of x and y location coordinates, an estimate of the accuracy of the location, the time the target was at the location coordinate, and a target classification. Multiple data points generated by the intersection of multiple LOBs originating from the same target are merged, using a modified AGNES clustering algorithm, into a single composite data point called a "measurement." The second process correlates prior scan measurements (called tracks) with current scan measurements using a sum-of-the-squares chi square gating technique. Each new data point forms two or more hypotheses:

- Hypothesis 1 is that the measurement is a new target data point not previously reported,
- Hypothesis 2 is that it is a false alarm (not a target at all), and
- Hypotheses 3 through n (where n is any integer greater than 3) is that the new data point "gates" (correlates) with one or more older target tracks generated on previous scans.

If the new measurement data are determined to be associated with a target track from a previous scan, the new measurement data are used to update the previous target track. The update is accomplished using a Kalman filter technique. The Kalman filter evaluates the new measurement data and their associated errors with the old target track data and associated errors, and decides how much the new measurement data will influence the old target track projected forward in time. Each hypothesis is scored based upon the "believability" of the data. A target track that is updated on subsequent scans is more "believable" than one that is not updated or one that is sporadically updated. Target tracks whose scores reach a pre-defined level are declared valid target tracks reported as such, and displayed on the CRT. A valid target track report includes the target's location, speed and direction, time of the report, and target classification. Figure 7 provides a top-level overview of the MHT architecture.

2.3.2 *Tracker Algorithms Using Multiple Hypothesis Logic with Extended Kalman Filter*

This tracking algorithm uses the sensor LOBs as the information source for the determination of target number and position. The algorithm attempts to isolate targets and maintain an account of their time history by grouping fixes into plausible target tracks, as illustrated in figure 8.

With each fix, the current estimate of the target's state is adjusted to better refine tracking accuracy. For the RNADS, the target states that are estimated are the target's x and y positions and velocity.

To accomplish these functions, the tracking algorithm can be partitioned into two parts: the track/measurement association logic and the track update process. These two algorithms have been designed and implemented. The difference between them is in the track/measurement data-association methodology.

One tracking algorithm uses a sophisticated data-association algorithm that formulates all possible measurement/track combinations each time a measurement set is received. This list of track combinations is combined into hypotheses that account for all plausible combinations of the sensor measurements. The hypotheses are scored each measurement cycle, and the tracks in the highest scoring hypothesis are designated the tracking

Figure 7. MHT with linear Kalman filter overview.

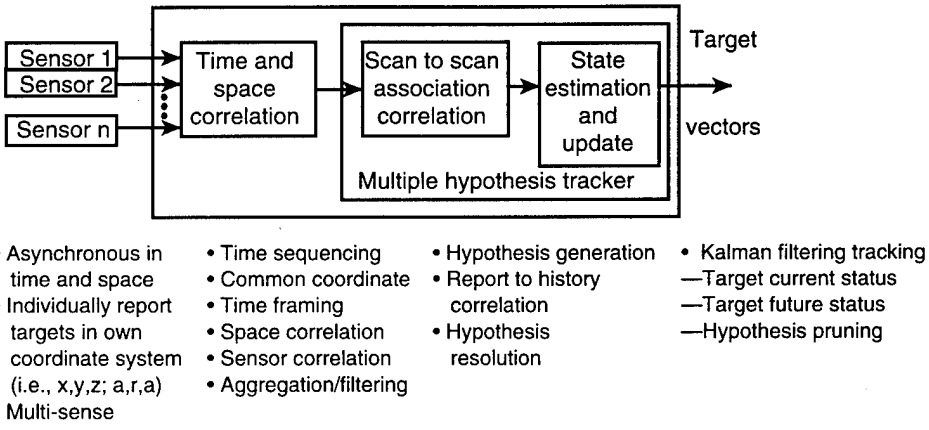

Figure 8. Hypothetical target tracks.

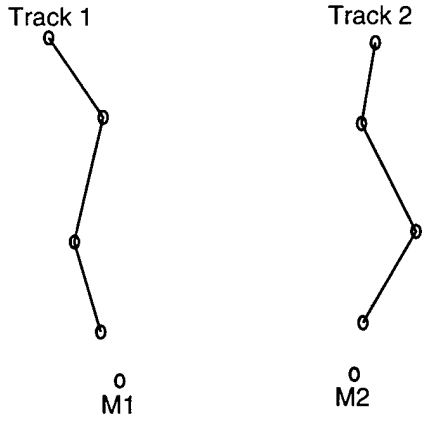

solution for that iteration. The strength of this data-association methodology is the ability to recover from a series of "bad" measurements. Since plausible tracks are maintained that are not a part of the top-scoring hypothesis, later measurement information can associate with these tracks and move them into the top hypothesis, if in fact they are the real target paths. This data association methodology, MHT, uses an algorithm presented by Reid in 1979 [1]. A top-level algorithm flow is shown in figure 9.

The second methodology is the nearest-neighbor data association. This technique seeks the unique pairing of measurements to tracks that optimize some scoring criterion across the entire pairing solution. With this algorithm, assignments are irrevocably made; the unique track solution set is carried forward without alternative solutions. The heart of this algorithm is the solution of the track/measurement assignment matrix. The matrix is formed by assigning a score for each measurement/track pairing. The score reflects the "distance" of the measurement from the track; low scores are given to measurements that lie near the track. Figure 10 shows an example assignment matrix. The 999 values reflect a measurement to track assignment that is implausible; the distance between track and measurement is so large that there is no probability that the measurement came from that track. The circled values are the optimal solution for this matrix; i.e., there is no set of pairings that sums to a lower total number. The code that is implemented in the nearest neighbor tracker to find the solution to the assignment matrix is based on a modified Munkres algorithm [2]. A top-level flow diagram is shown in figure 11.

The other portion of each of the tracker algorithms is the track update process. Once the data-association algorithm has made the measurement-to-track assignments, the track update process updates the estimates of each target's state (x and y positions and velocity) based on the measurement information. The algorithm that is used for this process is an extended Kalman filter.

The Kalman filter is a recursive algorithm that provides the optimal solution, in a mean-square error sense, to the linear system estimation problem. When the system is nonlinear, the extended Kalman filter algorithm must be used. In the case of acoustic tracking, the LOB measurements are a

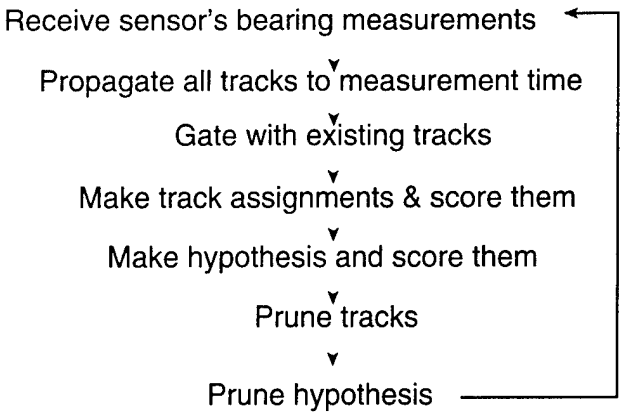

Figure 9. Multiple hypothesis algorithm flow.

Figure 10. Assignment matrix example.

	M1	M2	M3
Track 1	999	999	④
Track 2	999	6	6
Track 3	10	③	999
Track 4	6	8	7
Track 5	4	7	8
Track 6	11	4	999
Track 7	②	6	11

⇨ Track 1 with M3
Track 3 with M2
Track 7 with M1

Figure 11. Nearest neighbor algorithm flow.

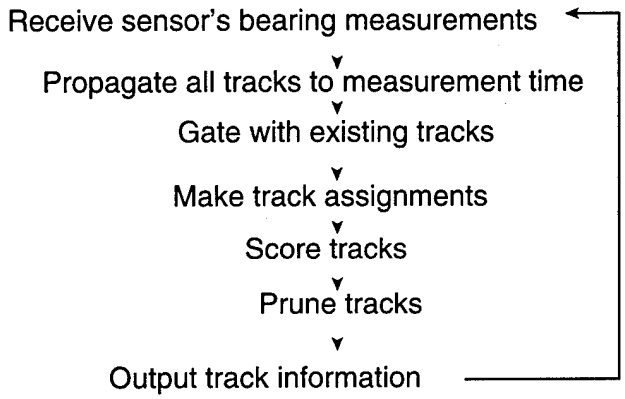

nonlinear combination of two of the states ($\tan^{-1}$ function of target x and y positions). The difference between the linear and extended Kalman filters is a linearization of the nonlinear system dynamics, or measurement equations in the extended case.

The discrete-time extended Kalman filter algorithm goes through the following steps every measurement cycle:

- The state estimate resulting from the last measurement is propagated to the time that the current measurement is received.
- The covariance of the state is propagated to the time that the current measurement is received.
- The filter estimate of the measurement value is computed based on the target state variables.
- The Kalman filter gain matrix is computed. The gain matrix is used to determine the portion of the difference between the actual measurement and the filter's estimate of the measurement that will be attributed to each state.
- The state estimate is updated by multiplying the gain by the difference in measurements and adding the result to the propagated state estimate.
- The covariance of the state is updated to reflect the measurement.

The measurement update equations (gain, state update, and covariance update) use a matrix that, when matrix multiplied with the state matrix, yields the filter estimate of the measurement. The geometry of figure 12 is used to define this matrix.

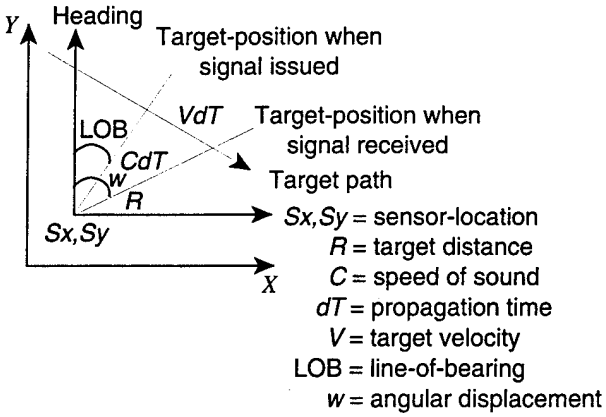

Figure 12. Acoustic measurement geometry.

3. Summary of Field Evaluations

Field evaluations were conducted at Aberdeen Proving Ground (APG), MD, and in Ze'elim, Israel. Three separate field evaluations were conducted at APG before the Israeli tests in order to verify equipment performance and characterize the sensors. The Israeli test consisted of two parts: a controlled experiment similar to the APG tests, and an uncontrolled test in which sensors were placed in a battlefield where wargame exercises were taking place. In the course of the field tests, a number of ground and air targets were used. The tests included ground vehicles and helicopters. Each field test was designed to evaluate the RNADS for single and multiple targets.

This chapter describes the field evaluations and the sensor and tracker performance. The first section describes the metrics used to measure sensor and tracker performance.

3.1 Performance Characterization

Performance metrics were developed to characterize sensor and tracker performance during the field tests.

3.1.1 Sensor Characterization

Sensor performance is characterized with the following quantitative metrics:

- Fixed angle bias
- Fixed time bias
- Random angle error
- Probability of detection
- Probability of multiple detections
- Probability of false target report

3.1.1.1 Computing fixed angle and time bias

Ground truth data were obtained for each field test run, with the exception of the Israeli uncontrolled test. Ground truth for the APG tests was gathered by noting the time at which the target vehicle(s) passed precisely located stakes along the closed course. For the Israeli controlled test, a GPS receiver on the vehicle provided the ground truth. An estimate of each sensor's fixed angle and time bias was computed by comparing reported sensor measurements with a computed estimate of "true measurement" values based on ground truth measurements. The true measurement values accounted for speed-of-sound propagation delays.

For fixed angle and time bias determination, false fixes were removed from the data. We eliminated these false fixes manually by comparing the measurement stream with the true measurement values. Figure 13 shows a plot of both sensor measurements and true measurements. The circled sensor measurements were removed to compute the bias values.

After false fixes are removed, the time bias is computed. The set of sensor and true measurements are differenced, and the average difference is found. This process is repeated with the sensor data set shifted in time. When the average difference is a minimum, the time shift is noted as the time bias. The angle bias is found in a similar manner. This time, however, the sensor measurement set is shifted in angle until a minimum average difference between the sensor and truth measurement set is found. The process used to determine time and angle bias is highlighted in figure 14.

3.1.1.2 *Computing random angle error*

After the time and angle bias have been removed from the sensor data, the random angular error is computed. The equation is

$$\text{Random bearing angle} = \sqrt{\frac{\sum_{i=1}^{i=N}\left(B_{T_i} - B_{M_i}\right)^2}{N-1}} \quad ,$$

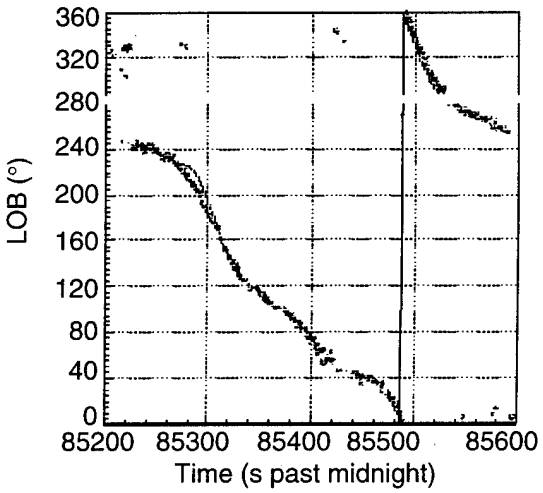

Figure 13. Typical sensor measurement evaluation.

Figure 14. Process used to determine time and angle bias.

where B_{T_i} is the true bearing at measurement time i, B_{M_i} is the sensor measurement at time i, and N is the number of sensor measurements.

The equation for the random error can be interpreted as the root sum square error, or the standard deviation.

3.1.1.3 *Computing other sensor characterization parameters*

The remaining sensor characterization parameters relate to the sensor's target detection capability. P_D is the probability, per reporting period, of detecting a target when the target is within sensor coverage. Sensor coverage for each run was determined manually by comparing sensor reports versus the true measurement line. Time periods when the sensor was providing measurements for the target were noted. The total number of reporting times that at least one target measurement is reported is then divided by the total number of seconds of sensor coverage, to yield P_D.

The probability that an LOB is for a false target, P_{FT}, is found by dividing the total number of false target reports by the total number of LOBs reported. Multiple reports of the target for one reporting time are not classified as false reports. They are counted, and the probability that a report is a multiple report of the target, $P_{MULTIPLE}$, is found by dividing the count by the total number of LOBs.

3.1.2 *Tracker Performance Metrics*

Tracker performance is a function of the number of sensors and their layout, accuracy of the sensor-provided LOBs, and target detection characteristics of the acoustic sensors. Since these characteristics changed from test to test, it is not possible to compare tracker performance across field tests. Comparisons can be made across runs within a test, however. The performance metric used was root sum square (RSS) tracker error from the ground truth. The computation is straightforward: For each tracker target position output (time, x position estimate, and y position estimate), the corresponding true vehicle position at the same time is computed from the ground truth data. The difference between true and estimated is squared, and the result summed with all other tracker outputs. The total summation is divided by the number of tracker outputs, and the square root of the result is computed.

This metric has a shortcoming. It does not penalize the tracker for losing track of the target; the computations are only made when the tracker has an estimate of target position.

3.2 Aberdeen Proving Ground, MD, 17 June–1 July 1992

This field evaluation was the first opportunity to integrate the acoustic sensors with the rest of the tracking system. Since this was the first full integration of the system, a number of software and hardware interface problems were discovered, which severely limited tracking capability.

Although tracking was not successful during the field test, this test provided the opportunity to identify interface problems. DAT recorders at each remote site allowed us to use data that were recorded during the field test to modify software and test new versions. This test also provided sensor placement, documentation, logistics, and test planning, which proved to be valuable on future field tests.

3.3 Aberdeen Proving Ground, MD, 21–30 October 1992

Another field test took place at the Aberdeen Proving Ground, to accomplish real-time tracking of single and multiple targets, and to gather data that would allow system performance characterization. Two additional sensor algorithms were developed: One algorithm used an alpha-beta tracking algorithm to group bearing fixes into tracks, and the other used an SVD algorithm. An objective of this set of tests was to determine the performance of each algorithm type.

3.3.1 Test Descriptions

Over the four-day test period of 26–29 October, 57 trials were conducted. For the trials involving ground vehicles, surveyed markers were placed around the closed course. Ground truth was generated by registering the time each marker was passed as the vehicle transited the course. For the helicopter trials, GPS data were collected.

Campbell Scientific meteorological stations were used to collect temperature, relative humidity, barometric pressure, wind speed, and directional data at several of the sensor sites and at the instrumentation trailer. Temperature, relative humidity, and barometric pressure were recorded each minute. Temperature and wind checks were made regularly and used to update the speed of sound estimations in the tracker.

3.3.2 Sensor Configuration

The course layout and sensor locations are shown in figure 15. Sensor positions 3A and 3B show alternative locations for one of the sensors. All trials except four were conducted with the sensor in position 3A. The last four trials were conducted with only sensor 3 operational (in position 3B). This set of tests was conducted to obtain additional long-range sensor data.

3.3.3 Sensor Performance

The sensor data for selected runs were reduced and grouped across runs by number and type of target for the run.

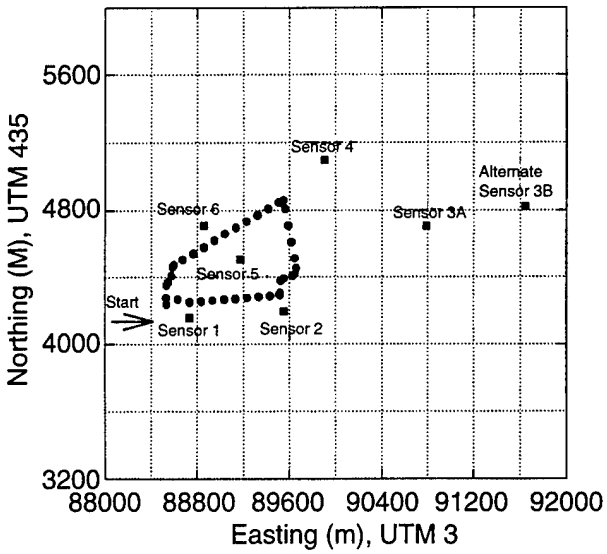

Figure 15. APG course and sensor configuration, October 1992.

Using the sensor characterization parameters described in section 3.1, the sensor performance for one-target runs using the alpha-beta sensor software was consistent in the time and angle bias values.

To gain further insight into sensor performance, the random angle error was binned by range-to-target in 100-m increments. The P_D, P_{FT}, and $P_{Multiple}$ results were consistent with other available systems. The random error was low for short range to target data, and remained low for the duration of the runs.

When the number of targets increases, the time bias, angle bias, and random error were found to be consistent with the single-target runs. For two-target runs, P_D was lowered only slightly, and the P_{FT} decreased. This reduction is most likely due to the sensor reporting a fixed number of LOBs. With additional targets in the sensor's field of regard, more real detections will occur and the false target statistics will drop.

3.3.4 *Tracker Performance*

3.3.4.1 *MHT with linear Kalman filter tracker performance*

Some very effective tracking was accomplished during the second test. Single vehicles were tracked nearly continuously around the 2.5-km track. The breaks in the track on the turns were caused by the sensors losing lock due to a sharp change in sound energy and frequency as the vehicle slowed to make the turn.

Multiple vehicles at appropriate spacing were tracked well. The target tracks had more breaks than in the single vehicle runs, but the correlation algorithms used did an excellent job at preventing the appearance of ghost tracks due to miscorrelation of sensor reports.

3.3.4.2 *MHT with extended Kalman filter tracker performance*

A number of runs were evaluated to determine the tracker RSS error. The errors for the single target runs ranged in values between the "loud" and "quiet" targets. Some sensors were not reporting information to the tracker during these runs; however, most of the tracking degradation was due to the lower signature of the target.

Tracker performance did not significantly degenerate on the two target runs. A sample plot of the tracks generated by the tracker for a typical run is shown in figure 16.

An example of the tracker output for a three-target run is shown in figure 17.

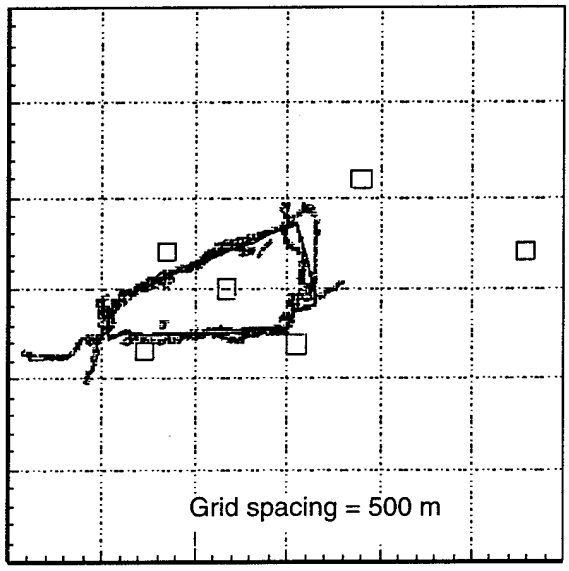

Figure 16. MHT with extended Kalman filter tracker—two-target run.

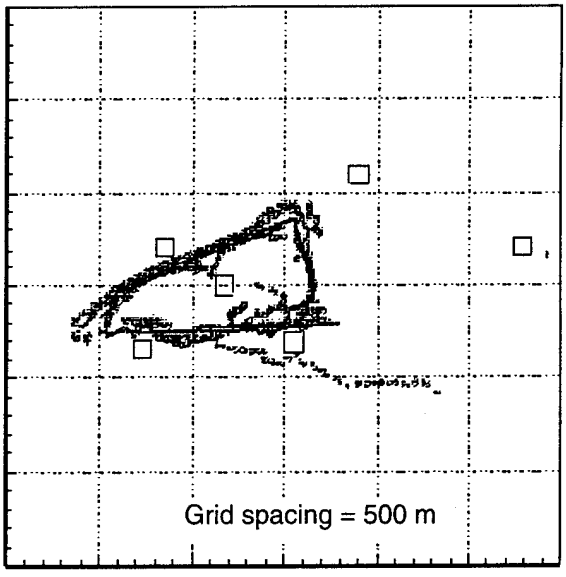

Figure 17. MHT with extended Kalman filter tracker—three-target run.

3.4 Aberdeen Proving Ground, MD, 28 January–3 February 1993

The final preliminary evaluation was used primarily to test additional pieces of equipment that had been constructed or received since the previous evaluation. Each piece of equipment planned for use in Israel was tested to ensure it was fully operational.

3.4.1 *Test Descriptions*

Five sensors were used in this set of field evaluations. A total of 16 single- and multiple-target trials took place. The time bias, angle bias, P_D, P_{FT}, and $P_{Multiple}$ calculations were consistent with previous tests.

3.4.2 *Tracker Performance*

The various trackers yielded results similar to the previous tests when vehicles were appropriately separated.

3.5 Field Evaluations, Ze'elim, Israel, 1–18 March 1993

The demonstration of the RNADS was conducted in Israel in conjunction with a brigade-level training exercise. This evaluation consisted of two parts. The first part was a controlled test similar to the evaluations conducted at Aberdeen Proving Ground, MD. Test targets for this evaluation included ground vehicles and helicopters. The second portion of the evaluation was an uncontrolled test, with the sensors placed along the perimeter of battalion- and brigade-level exercise areas.

3.5.1 *Controlled Test*

The controlled test was conducted on a triangular course with the sensors more widely spaced than in previous tests. The remote processing setup was in a control tower near the start of the course. Nine sensors were used. The geometry is shown in figure 18.

During the controlled test, the background noise level at the sensors was high due to power generators near the control tower. Sensors detected these generators as stationary sources.

A number of single and multiple targets were used at varied speeds for these experiments. Target spacing varied from 100 to 500 m.

3.5.1.1 *Sensor performance*

The sensor data for each run were reduced and grouped across runs by number and type of target for the run. A representative set of sensor measurements and associated ground truth is shown in figure 19.

Figure 18. Sensor configuration for controlled test in Ze'elim, Israel.

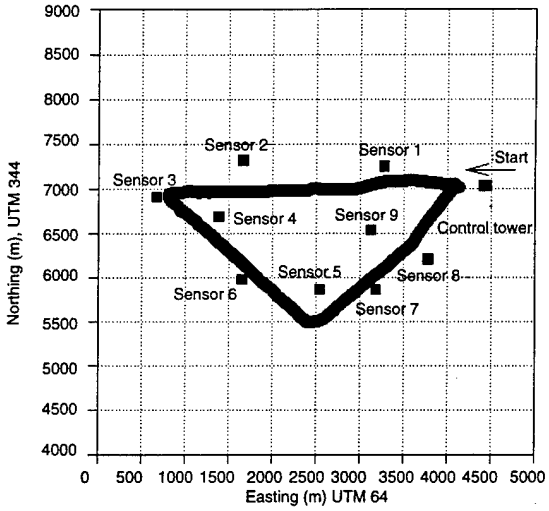

Figure 19. Representative sensor data.

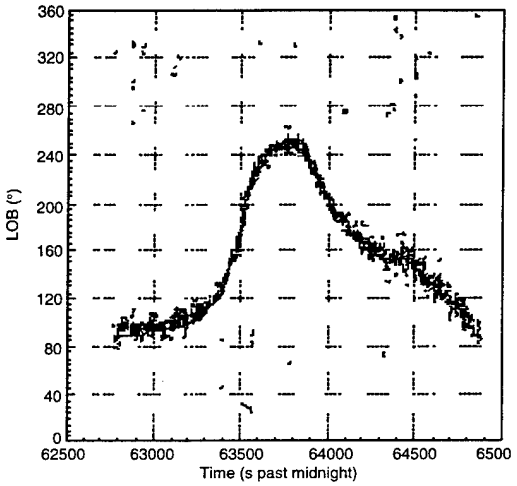

Sensor performance for single-target runs.—A total of 33,518 LOBs were analyzed from eight sensors to determine P_D, P_{FT}, $P_{Multiple}$, time bias, angle bias, and random error. Comparison of these with the Aberdeen results leads to the following conclusions:

- The magnitude of the time bias is approximately the same as that experienced at Aberdeen, but the variance among sensors is greater in the Israeli tests.
- The magnitude of the random error is larger in these tests than it was at Aberdeen. The cause of this discrepancy is likely due to the adequacy of the ground truth.
- P_D closely matched the Aberdeen results.
- P_{FT} was higher than in the Aberdeen results. A partial cause of this discrepancy is a number of low-level aircraft passing the test site to the west.
- $P_{Multiple}$ was also higher than it was at Aberdeen. It is thought that this increase is a by-product of the increase in the maximum number of LOBs

that each sensor could report: an increase from three at Aberdeen to eight in Israel. The percentage of LOBs contained in the multiple reports is greater than the percentage of single-LOB report LOBs.

As was the case during the Aberdeen tests, sensor performance dropped off for the less observable target.

For the Aberdeen runs, random error was more accurate at 100 to 200 m range-to-target; leveled off, and increased from there until the target was out of detection range. In the Israeli test, the random error is higher at ranges-to-target less than a few hundred meters. It is this large error that causes the overall random error to be higher than the Aberdeen. The cause of this large error at shorter ranges-to-target is attributed to GPS ground truth error. The GPS used on the targets were accurate to within 100 m. Figure 20 shows the number of degrees of sensor error that inaccurate ground truth can introduce.

P_D as a function of target range was calculated for 300 to 2600 m ranges for the single-target runs. Sensor reported LOBs-on-target were binned by range-to-target in 100-m increments. The number of LOBs that should have been reported for each range bin were computed from the ground truth. The results were comparable to the APG field experiment.

The typical P_D versus range plot showed a high probability of detection at close ranges, and a gradually decline as the range increases.

Sensor performance for two-target runs.—The two-target P_D is lower than the single-target value, while the two-target P_{FT} is better than the single-target value. Again, the single-target runs have a number of aircraft targets in the vicinity which the sensors did track.

The two-target runs show a higher random error than was the case for the one-target. P_D is also greatly reduced. The large P_{FT} value can be attributed to background and interfering sources such as the generators.

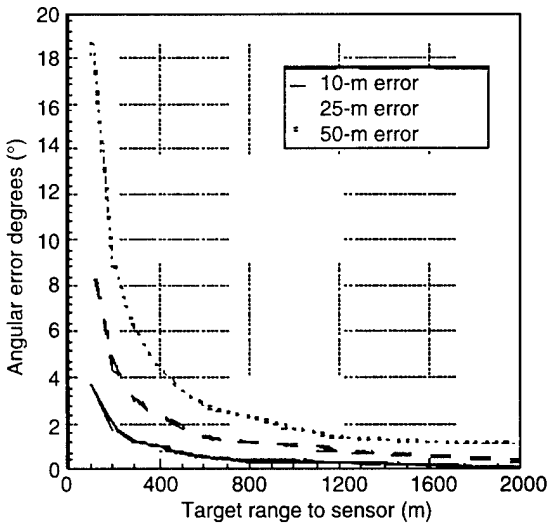

Figure 20. Random error versus target range.

3.5.1.2 *Tracker Performance*

MHT tracker with linear Kalman filter performance.—The first set of tests was conducted using a single target. Excellent tracks were maintained along each leg of the course. Target tracks were fairly close to the road that the vehicle traveled on. The targets had to stop at each corner for safety reasons, so the tracks were frequently broken at that point. The second leg of the course was very hilly with numerous short but very steep hills. We feared that the sensors would have problems maintaining a lock on the tanks as their speed changed going up and down the hills; however, sensors maintained consistent reporting. Figure 21 shows a single target being tracked by eight acoustic sensor arrays, displayed as black boxes. The white line is the ground truth obtained using a commercial GPS receiver, and the jagged black line is the output of the tracker.

The next set of tests were with two targets with varying separation. Similar results were achieved here as were achieved at APG. The targets had problems maintaining their separation and frequently ended up less than 100 m apart. Tracking was more difficult during these times. Figure 22 shows the tracking of two similar targets.

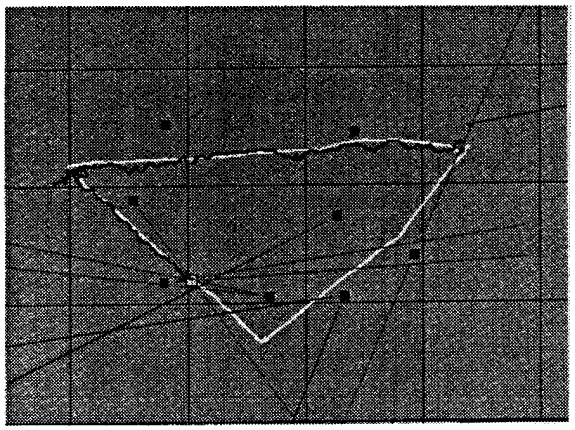

Figure 21. MHT tracker with linear Kalman filter—eight sensors reporting, one target, 1-km grid.

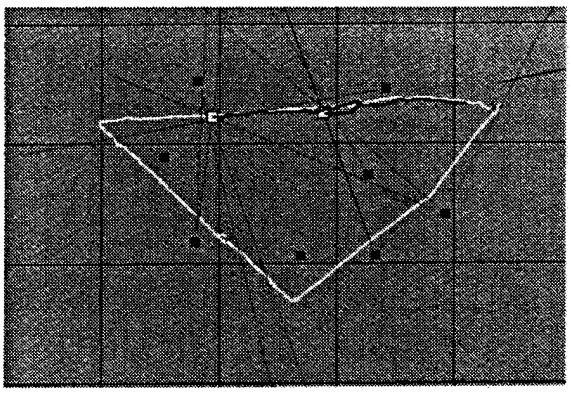

Figure 22. MHT tracker with linear Kalman filter—eight sensors reporting, two targets, 1-km grid.

For tests involving multiple vehicles, the tracks were generally better on the more pronounced signatures. Quieter targets broke track more frequently. As expected, good tracks resulted when sensor performance was good.

MHT tracker with extended Kalman filter performance.—For the Israeli test, the nearest-neighbor tracking algorithm was used. Pretest analysis pointed out that with up to nine sensors reporting, the multiple hypothesis algorithm would not run in real time with more than three or four LOB reports per sensor.

The tracker RSS error and tracking percentage were calculated for a number of single- and two-target runs. The RSS error was calculated after removing the GPS bias, which was calculated by averaging the GPS-indicated target position and tracker-indicated target position for the same reporting times. The validity of the computation rests on the assumption that the tracker output is unbiased. Analysis of the Aberdeen tests shows the tracker to be unbiased.

The results show the expected trends: Single-target runs are better than two-target runs of the same type; tracking accuracy against the less observable second target was not as good as against the first target; and tracking percent drops as number of targets increases and observability decreases. The general conclusion that can be drawn is that tracking performance follows sensor performance.

3.5.2 *Uncontrolled Test*

The uncontrolled portion of the evaluation was conducted in two parallel battalion-sized attack corridors about 8 km long. The two corridors, one 3 km wide and the other 4 km wide, were divided by a road. Three sensor sites were set up along the road at approximately 2 km spacing. Three more sensors were set up along each of the outside edges of the corridors. See figure 23 for the layout of this exercise. Since the Israeli army was conducting live-fire training, the sensors had to be set up well in advance of the evaluation period. By the start of the maneuver exercises, only six sen-

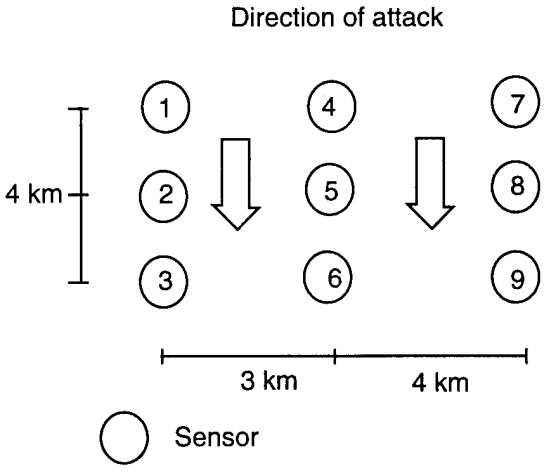

Figure 23. Sensor layout for uncontrolled exercise.

sor sites remained operational. Three sensors were down before the exercise was started. Attempts to restart the sensors from the central command site were unsuccessful.

The planned maneuver exercises included one battalion-sized armor unit moving down each corridor (one battalion at a time), while conducting live-fire training. This was to be followed by a battalion on battalion maneuver in one of the corridors. The actual movement and timing of the exercises is not known. No ground truth was provided and the maneuver area was not within sight of the control tower; therefore exact target positioning is unknown during these experiments.

We made an attempt to develop tracks with the paucity of data by adjusting the MHT parameters of the linear Kalman filter tracker. Although several tracks were formed, it appeared that in most cases the tracks formed were the result of miscorrelations and ghost tracks. Only the closest one to three targets to the sensor generated a sufficient SNR to be detected and processed. No two sensors were detecting the same targets at the same time. Since the linear Kalman filter MHT algorithm is based upon triangularization of LOBs from geographically dispersed sensors hearing the same target, conditions for tracking were not satisfied.

The nearest-neighbor tracker was capable of showing the general directional flow of the column of vehicles; however, in general tracking was poor. Additional analysis using data from a controlled test with good ground truth is necessary to determine sensor and tracker performance.

4. Conclusions

The RNADS has been successfully demonstrated at field tests within the U.S. and outside the U.S. as part of a demonstration for the Israeli government. Real-time passive x-y tracking has been demonstrated with good accuracy for multiple vehicles. The following conclusions are drawn from the sensor and tracker analysis performed:

(1) Sensor performance and tracker performance were shown to be good for single targets, and both begin to degrade as the number of targets increase. P_D would drop several percentage points when an additional target is added. How much the value dropped often depended on background conditions and interfering sources. P_{FT} would usually decrease when additional targets are within the field of regard. With another target in the sensors' field of regard, the sensors reported less false fixes. The tracker performance followed the general trend of the sensor performance. RSS error and tracking percentages were shown to decrease with increased targets for all targets observed.

(2) As the targets become less separated, the sensors had more difficulty resolving the targets and tracking performance suffered.

(3) A time bias was found within the sensors. The data characterization allowed for the removal of this time bias in processing to provide better tracking. The cause of the bias is believed to be sensor-processing related.

(4) An angle bias in the sensors was determined to be due to sensor layout. This can be easily compensated for within the tracking algorithms. Careful placement of the microphones within the array minimizes this bias. Knowing the magnetic deflection in the area also eliminated compass-read errors and sensor-placement errors.

(5) The sensor-random error was found to be fairly consistent for most test ranges.

(6) As expected, P_D was shown to degrade with increasing distance. For the controlled experiments and tests around closed paths, quite often, the P_D would drop dramatically at certain points along the path. These distances were determined turn points, where the target would slow to maneuver. When the engine decreased rpms, the overall signature became less observable and detection probability dropped.

(7) As the number of targets increased dramatically, as was the case in the Israel uncontrolled experiment, sensor and tracking performance degraded to the point where, at times, only the general direction of flow could be determined. Only the loudest and closest targets to the sensors were tracked for short periods. Due to the distance between operational sensors, correlation of LOBs between sensors was difficult. The lack of ground truth prevented formal data characterization and performance analysis on these data. Additional data are required to characterize sensor and tracker performance as the number of targets increase past three or four.

(8) The goals and objectives of this project were fulfilled. The program developed, enhanced, and integrated a set of sensor and tracking algorithms needed to provide tracking in a multiple-target environment. These algorithms were demonstrated during field tests within the U.S. and overseas as part of a U.S.-Israel joint technology demonstration program. Also, the database of single and multiple targets was increased. This database includes a complete set of ground truth data, including meteorological and positioning data for multiple environmental and background noise conditions.

(9) Acoustic sensors provide a unique capability not found in conventional-based sensors. They provide an inexpensive and excellent adjunct to conventional sensor systems. They provide passive non-line-of-sight detection and tracking capabilities not possible with radar-type systems.

5. Recommendations

The design and testing of the RNADS system was challenging. Meeting and fulfilling the objectives of this project were possible only because of the cooperation and dedication of many agencies and contractors. The following are recommendations from this team for system enhancements for future applications and growth:

(1) Integrate the acoustic-processing hardware and the communications-processor hardware into one ruggedized, weatherproof container to increase portability and reduce logistics problems. The overall system is bulky and difficult to transport from site to site.

(2) Upgrade the radio communications system to reduce radio interface and communication difficulties. When a sensor became inoperable, it was quite often due to the radio link between the remote sensor and the tracker. The problem was believed to be in the HDLC interface or the radio itself. Additional analysis is recommended to determine the cause of the communications problem and the recommended replacement system.

(3) Modify the sensor configuration to allow the incorporation of additional sensor types. Currently the sensor uses acoustic sensors. Adding the capability to place other sensors such as seismic, magnetic, or infrared (IR), may enhance the system capability and flexibility to expand application possibilities.

(4) Conduct a set of controlled experiments using multiple targets with ground truth to determine sensor and tracker performance as the number of targets increases. These tests should be designed to determine optimal sensor configurations and target separation.

(5) Routinely conduct sensor characterization along with field tests. Metrics calculated in this report allowed a better understanding of the sensors. These data were used to improve tracker performance, as well as to modify sensor algorithms.

Acknowledgment

We regret that Dr. Norman J. Berg is no longer alive to witness the issue of this report. Dr. Berg initiated the concept of networking acoustic sensor arrays in the battlefield to generate, in real time, the x,y coordinates of detected targets. He was a pioneer in the field of acoustics and strived to enhance the state-of-the-art of this technology. This project was initiated in the winter of 1991. Over the following two years, a rigorous effort was put forth by ARL and its supporting contractors to build hardware, write software, and conduct three field experiments at APG to evaluate the performance of the system. The goal was to conduct a full-scale joint field experiment with the Israeli Army to demonstrate the capability of the U.S. acoustic detection system. We are thankful that Dr. Berg lived long enough to witness the success of the Israeli field test in March 1993. He has left a void at ARL and we will surely miss him.

References

1. D. B. Reid, "An Algorithm for Tracking Multiple Targets," IEEE Transactions on Automatic Control, **AC-24**, pp 843-854 (December 1979).

2. F. Burgeois and J. Lassalle, "An Extension of the Munkres Algorithm for the Assignment Problem to Rectangular Matrices," Communications of the ACM, **14**, pp 802-806 (December 1971).

3. R. Tenney and J. Delaney, "A Distributed Aeroacoustic Tracking Algorithm," Proceedings of the American Control Conference (June 1984).

Acronyms

A/D	analog-to-digital converter board
ARDEC	Army Armament Research, Development, and Engineering Center
ARL	Army Research Laboratory
CECOM	Army Communications-Electronics Command
CP	communications processor
DAT	digital audio tape
DSP	digital signal processing
EPROM	erasable programmable read-only memory
FFT	fast Fourier transform
GPS	Global Positioning System
HL	harmonic line
HLA	harmonic line association
IITRI	IIT Research Institute
LOBs	lines of bearing
LPR	low-cost packet radio
MAP	maximal a posteriori
MHT	multiple hypothesis tracker
NCPF	network control processing facility
PC	personal computer
RAM	random-access memory
RNADS	Remote-Netted Acoustic Detection System
RSS	root sum square
SNR	signal-to-noise ratio
SS&H	simultaneous sample and hold
SURAN	Survivable Radio Network
SVD	singular value decomposition
SVP	sound velocity profile

Distribution

Admnstr
Defns Techl Info Ctr
Attn DTIC-DDA (2 copies)
Cameron Sta Bldg 5
Alexandria VA 22304-6145

AATD (ATCOM)
Attn AMSAT-R-TU L Sutton
FT Eustis VA 22604

ARDEC
Attn SMCAR-FSF-RM W Donnally
Bldg 95N
Attn AMSTA-AR-FSF-R J Heberley
Bldg 95N
Attn SMCAR-FSM-W K Wong
Bldg 94N
Picatinny NJ 07801

Joint Tactical Missile Defense
US Army Missile Command
Attn V Armbruster
Redstone Arsenal AL 34898

MICOM
Attn AMSMI-RD-SS-AA R E Alongi
Redstone Arsenal AL 34898-5254

NVESD
Attn AMSEL-RD-NV-GSID J Brooks
FT Belvoir VA 22060

US Army AFDD
Attn AMSAT-R-AF D Boxwell
Ames Rsrch MN N215-1
Moffett Field CA 20301-1001

US Army ATCOM Natick RDE Ctr
Attn SATNC-YBH J Sampson
Natick MA 01760-6000

US Army Belvoir RD&E Ctr
Attn SATBE-NAD R Stanfield
FT Belvoir VA 22062-5606

US Army CECOM
Attn AMSEL-LC SM S3 M Dipaola
Attn AMSEL-RD-NV-CI-NCTF L Stein
FT Monmouth NJ 07703-5017

US Army CECOM/NVESD
Attn AMSEL-RD-NV-RD-IFF M Muller
FT Monmouth NJ 07703

US Army CERDEC, NVESD
Attn AMSRL-RD-NV-VISP-CR G Klager
FT Belvoir VA 22060

US Army CSTA
Attn STECS-AC-C G Rogers
Attn STECS-EN-PS R Joy
Aberdeen Proving Ground MD 21005

US Army Ctr for Health Promotion
Attn HSHB-MO-B G A Luz
Aberdeen Proving Ground MD 21010-5422

US Army INSCOM
Attn IAOPS-MA-S B Meyer
8825 Beulah Stret
FT Belvoir VA 22060-5246

US Army Mis Cmd RDEC
Attn RFPI E Van Dyver
Redstone Arsenal AL 35898

US Army Mis Cmnd Weapons Syst Mgmt
Attn M Harris
Redstone Arsenal AL 35898

US Army NVESD
Attn AMSEL-RD-NV-UAB C Walters
10221 Burbeck RD
FT Belvoir VA 22060

US Army Rsrch Lab/BED
Attn AMSRL-BE-S D Marlin
White Sands Missile Range NM 88002

Distribution

Commander
US Army Rsrch Ofc Durham
Attn M Ciftan
Research Triangle Park NC 27709

US Army TACOM
Attn AMSTA-TR-S E Shalis
Attn AMSTA-JCS D Thomas
Warren MI 48090

Commander
USAE Waterways Experimental Station
Attn CEWES-SE-R B Carnes
3909 Halls Ferry Rd
Vicksburg MS 39180-6199

White Sands Missile Range
Attn J E Noble Chief Land Sys Br
Bldg 1530
White Sands Missile Range NM 88002

Nav Undersea Warfare Ctr
Attn Code 2141 D Wilson
Attn Code 2141 M Peloquin B80/RM
Attn Code 2143 J Marsh
New London CT 06320

Commander Officer
NSWC
Attn G Gaunaurd
10901 New Hampshire Ave
Silver Spring MD 20904

Ofc of Nav Rsrch ONR 322AM
Prgm Mgr Atmospheric Modeling
Attn S A Sandgathe
800 M Quincy RM 428 BCT
Arlington VA 22217-5660

Chick Ltl Jnt Proj
Attn 46 OG/OGML J A Sledge
104 Cherokee Ave
Eglin AFB FL 32542-5600

Department of the Army
US Military Academy
Attn D/C&ME M Costello
Westpoint NY 10996-1792

Appld Rsrch Lab
Attn M B Bennett
PO Box 8029
Austin TX 78713-8029

Appld Rsrch Lab
Penn State Univ
Attn D C Swanson
Attn K Gilbert
PO Box 30
State College PA 16804

Georgia Tech Rsrch Inst
Rsrch Security Dept
Attn J Echard
Atlanta GA 30332

ITT Defns
ITT Arspc/Commctn Div
Attn P A Gilmour
100 Kingsland Rd
Clifton NJ 07014-1993

Keweenaw Rsrch Ctr
Michigan Tech Univ
Attn J Rogers
1400 Townsend Dr
Houghton MI 49931

University of Mississippi
Attn H E Bass
NCPA
University MS 38677

260SF
Attn E Nilsen
Unit 8995 Box 545
APO AE 09094

AT&T Bell Labs
Attn C De Haven
67 Whippant Rd RM 15H-324
Whippany NJ 07981

Distribution

CSC
Attn W Greenleaf
4815 Bradford Dr
Huntsville AL 35805

IIT Rsrch Inst
Attn J Robertson (10 copies)
4140 Linden Ave Ste 201
Dayton OH 45432-3034

IITRI New Mexico Technology Center
Attn M Conlon
2509 N Telshor Blvd
Las Cruces NM 88011-8222

Lockheed Sanders Inc
Attn S W Lang
PO Box 2057
Nashua NH 03061-0868

McDonnell Douglas
Attn B Jackson
PO Box 516 M/C 064-2206
ST Louis MO 63166

MCQ Assoc Inc
Attn D Rich
1551 Forbes Stret PO Box 8322
Fredericksburg VA 22405

MIT Lincoln Lab
Attn R Lacoss
244 Wood Stret PO Box 73
Lexington MA 02173

NCCOSC RDT&E Div
Attn Code 7502 G Dobson
San Diego CA 92152

Nichols Rsrch Corp
Attn S Wolfenbarger
4040 S Memorial PO Box 40002
Huntsville AL 35815-1502

Northrop Corp
Attn Y-M Cheng
PO Box 5032
Hawthrone CA 90251-5032

Riverside Rsrch Inst
Boston Rsrch Office
Attn R L Hernandez
70 Westview Stret Kilbrook IV
Lexington MA 02173

RTA
Attn J Brush
PO Box 5267
Springfield VA 22150

Sandia Labs
Attn G Haschke
Attn L Stotts
Albuquerque NM 87185

SNL
Attn J Rhines
1380 Berryville Rd
Germantown MD 20874

SRI Internation Appld Electromagnetics
and Optic
Attn R Abileah
333 Ravenswood
Menlo Park CA 94025-3493

TASC
Attn D Fruit
1992 Lewis Turner
FT Walton Beach FL 32547

US Constrctn Engrg Rsrch
Attn L L Pater
Attn M White
PO Box 9005
Champaign IL 61826-9005

Distribution

USANGIC
Attn IANGIC-RSG B Grachus
220 7th Stret NE
Charlottesville VA 22973

CIA Central Intelligence Agency
Attn J Croce
Washington DC 20505

NASA Langley Research Center
Attn AMSRL-VS-L D Hoad
Hampton VA 23681-0001

Army Rsrch Lab HRED
Attn AMSRL-HR-SD G Garinther
Aberdeen Proving Ground MD 21005

Army Rsrch Lab/SLAD
Attn AMSRL-SL-EV R Velasquez
White Sands Missile Range NM 88002

Army Rsrch Lab/WTD
Attn AMSRL-WT-WG P Kaste
Aberdeen Proving Ground MD 21005

Director
US Army Rsrch Lab
Attn AMSRL-HR-SD J Kalb
Aberdeen Proving Ground MD 2105-5425

US Army Rsrch Lab
Attn AMSRL-SE-EA N Srour (10 copies)
Attn AMSRL-LT G Roffman
Attn AMSRL-OP-SD-TA Mail & Records Mgmt
Attn AMSRL-OP-SD-TL Tech Library (3 copies)
Attn AMSRL-OP-SD-TP Tech Pub
Attn AMSRL-SE-EP M Scanlon
Attn AMSRL-SE-EP S Tenney
Adelphi, MD 20783-11967